Date of publication xxxx 00, 0000, date of current version xxxx 00, 0000.

Digital Object Identifier 10.1109/ACCESS.2017.Doi Number

Magnetic Equivalent Circuit Model for Performance Prediction of Two-DOF Planar Resolver

F. Zare [1], F. Tootoonchian [2], Senior Member, IEEE, A. Daniar[3], M. C. Gardner[3], Member, IEEE, and B. Akin[3], Fellow Member, IEEE

[1]Department of Electrical and Computer Engineering, Isfahan University of Technology, Isfahan, Iran
[2]Department of Electrical Engineering, Iran University of Technology
[3] Electrical Engineering Department, The University of Texas at Dallas, Richardson, TX

Corresponding author: Matthew Gardner (matthew.gardner@utdallas.edu)

This work is based upon research funded by Iran National Science Foundation (INSF) under project No. 99026258

ABSTRACT In this paper, an analytical model based on the Magnetic Equivalent Circuit (MEC) method is developed for a planar wound mover two-degree of freedom (2-DOF) resolver. Planar resolvers enable mass, volume, and complexity reductions for position control of 2-DOF linear actuators. However, similar to any other linear electromagnetic sensors, the performance of the planar resolvers is negatively affected by the limited dimensions of the mover's ferromagnetic core. Thus, it is necessary to develop an appropriate compensation method. On the other hand, the 3-D geometry of the sensor necessitates extremely time consuming 3-D time-stepping analysis. Therefore, a fast yet accurate analytical model is critical for the iterative design and compensation algorithm. In order to address these modeling limitations, the slot-tooth region and longitudinal end effect are included in the model. Then, its accuracy is verified by comparing the results with those of the 3-D time stepping finite element method (TSFEM). Then, the developed model is employed for design optimization to compensate for the end effects. Finally, the optimal sensor is experimentally prototyped and tested.

INDEX TERMS Two-DOF Resolver, Linear Resolver, Wound Mover Resolver, Longitudinal End Effect, Magnetic Equivalent Circuit (MEC)

NOMENCLATURE

Symbol	*Definition*
g	*The air-gap length*
l	*Length of Mover/Stator*
w_{ST}	*Stator tooth width*
h_{ST}	*Stator tooth height*
h_{SY}	*The height of stator yoke*
ρ_{ST}	*Equivalent permeance of stator tooth*
ρ_{SYx}/ρ_{SYy}	*Equivalent permeance of stator yoke in x /y direction*
ρ_{SY}	*Equivalent permeance of stator yoke*
ρ_{SS}	*Equivalent permeance of stator slot*
w_{MT}	*Mover tooth width*
w_{ST}	*Stator tooth width*
h_{MY}	*The height of mover yoke*
ρ_{MT}	*Equivalent permeance of mover tooth*
ρ_{SMx}/ρ_{SMy}	*Equivalent permeance of mover yoke in x /y direction*
ρ_{SM}	*Equivalent permeance of mover yoke*
ρ_{SM}	*Equivalent permeance of mover slot*

I. INTRODUCTION

Accurate and reliable position calculation is an essential part of motion control in automotive, electric vehicles (EVs), and robotic applications [1]. Increasing deployment of two-degree of freedom (2-DOF) electrical machines in recent years necessitates accurate 2-DOF position sensors. 2-DOF electrical machines are divided into two main groups according to their motion, rotational-linear (helical motion machines) and planar x-y linear machines. Accordingly, two types of 2-DOF position sensors are possible, helical motion and planar x-y linear motion sensors. Using a 2-DOF planar sensor as an alternative for two single DOF sensors reduces the complexity, volume, and mass of the control system [2]. Among different types of position sensors, resolvers are highly attractive for their robustness in most harsh environments [3]-[4].

Various papers have studied helical motion resolvers [5]-[6]. However, 2-DOF planar electrical machines, which are used in x-y Tables, pantograph type planar robots [7], scanning probe microscopes, and optical fiber alignments [8], need the mover position measured in two perpendicular directions of linear motion. Different types of linear position sensors are proposed in the literature [9]-[12], and the concept design for the 2-DOF linear resolver is presented in [12] for the first time. However, no analytical method is reported in [12]. Instead, [12] relies on trial and error using finite element analysis to design the resolver. Therefore, in this paper an analytical method based on a magnetic

© IEEE 2023

equivalent circuit (MEC) for the planar resolver is proposed to reduce the computational burden. The developed model is modified to include the longitudinal end effect. After verifying the model's accuracy, it is used to compensate for the influence of the finite dimensions of the mover. In addition, the proposed model, can be used to determine the influence of sensor's physical parameters on the performance of the resolver. Finally, the compensated sensor is built and tested. Close agreement between the simulation and the experimental results shows there is only a 0.011% of pole pitch difference between the average of absolute position error (AAPE) of the proposed model and the experimental results, which confirms the successful application of the proposed model and compensation method.

II. STUDIED CONFIGURATION

The studied resolver has a flat, planar configuration. Fig.1 shows the mover, which has two sets of perpendicular slots containing two excitation windings. The flux produced by each excitation winding is used for detecting the motion in one direction. On-tooth variable turn configuration, which is shown in Fig. 2, is used for the excitation winding to achieve a more sinusoidal distribution of the excitation flux and avoid half-filled slots in the sensor's ends, which would produce a static end effect. It is worth mentioning that the positive/negative number of turns shows the direction of the winding coils.

Sixteen slots are devoted to each DOF in the studied configuration. The number of mover slots correlates with the stators' number of slots and the windings' pole number. A 2-pole configuration is selected because 2-pole resolvers can be used in the control loop of the machines with different pole numbers and give the absolute position information. Thus, the studied resolver is a single-speed resolver. The optimal mover/stator teeth combinations for single-speed resolvers include 36/12, 20/11, 20/12, and 16/12 [13]-[14]. A higher number of slots usually lead to higher sensor accuracy [15] but generally increases winding complexity and the resolver's size. Based on these considerations, the combination of 16 slots/teeth for the mover and 12 slots/teeth for the stator modules are employed for this design.

Like the mover, the stator has perpendicular slots containing 2-phase signal windings for each direction, shown in Fig. 3. The distribution of the signal windings is given in Fig. 4. For linear motion, either the stator or mover must be longer than the other. As the stator has a larger slot pitch, the stator is selected to be the longer part and is built using three identical modules.

III. PROPOSED ANALYTICAL MODEL

Although the finite element method is the most accurate way to simulate resolver performance, it is too slow for iterative design studies. Hence, we propose an analytical model to address the end effect problem and then compensate for it in a two-DOF planar resolver.

To develop a MEC model for the studied resolver, it is required to determine the equivalent permeances of each part.

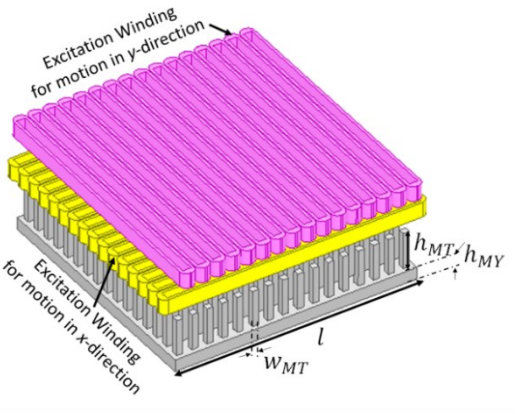

FIGURE 1. The mover of studied resolver

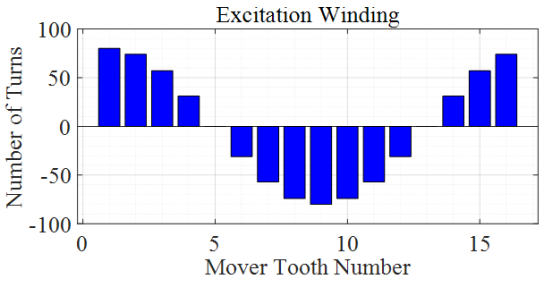

FIGURE 2. The distribution of the excitation winding for the studied mover

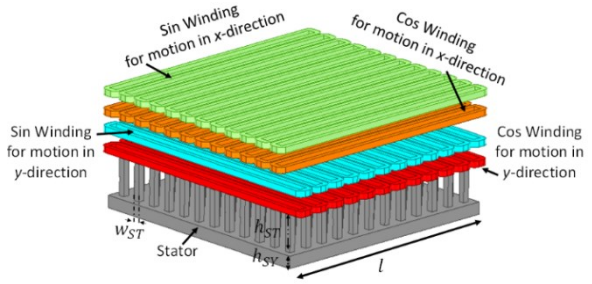

FIGURE 3. The configuration of each stator module of the studied resolver

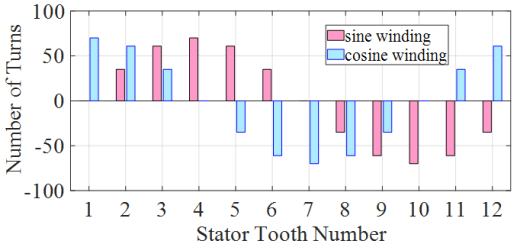

FIGURE 4. The distribution of the signal windings of studied resolver

Because the resolver functions as a sensor with negligible output power, it always operates in the linear part of the B-H curve and much below the saturation point (Fig. 5). Therefore, the proposed model is linear, where the relative permeance of each element is always a constant value. This makes the model fast without significantly degrading its accuracy. The proposed MECs of the mover and the stator are given in Figs. 6(a) and (b), respectively. The air-gap permeances, as the most significant permeances of the MEC model, are shown in Fig. 7.

The permeance of each stator tooth (Fig. 6(b)), ρ_{ST}, can be calculated as

$$\rho_{ST}=\frac{\mu_0\mu_r w_{ST}^2}{h_{ST}} \tag{1}$$

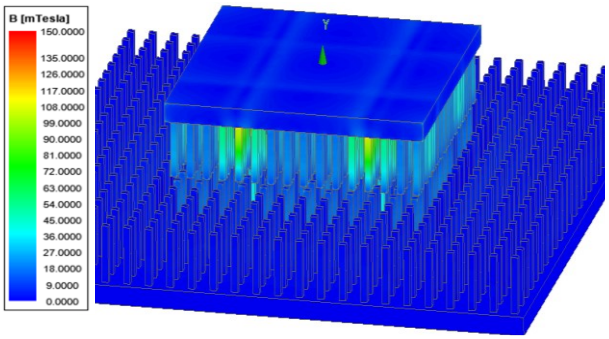

FIGURE 5. The spatial variation of magnetic flux density over the surface of the sensor's body

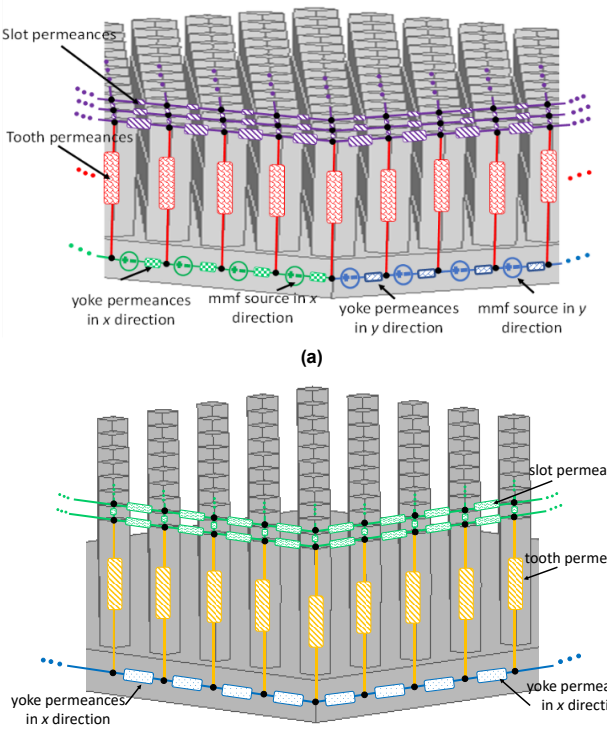

FIGURE 6. The proposed MEC model for the studied resolver: (a) mover, and (b) stator

Similarly, the stator yoke permeances, ρ_{SYx} and ρ_{SYy}, can be calculated as:

$$\rho_{SYx}=\frac{\mu_0\mu_r h_{SY} N_{Sx}}{N_{Sy}} \tag{2}$$

$$\rho_{SYy}=\frac{\mu_0\mu_r h_{SY} N_{Sy}}{N_{Sx}} \tag{3}$$

where N_{Sx} and N_{Sy} are the number of stator slots in the x and y directions, respectively. Considering the symmetry of the stator geometry,

$$N_{Sx}=N_{Sy} \tag{4}$$

$$\rho_{SY}=\rho_{SYx}=\rho_{SYy}=\mu_0\mu_r h_{SY} \tag{5}$$

The stator slot permeance can be calculated as

$$\rho_{SS}=\frac{\mu_0 h_{ST} w_{ST}}{\frac{l}{N_S}-w_{ST}} \tag{6}$$

The mover tooth permeance can be calculated as

$$\rho_{MT}=\frac{\mu_0\mu_r w_{MT}^2}{h_{MT}} \tag{7}$$

The mover yoke permeance is

$$\rho_{MY}=\mu_0\mu_r h_{MY} \tag{8}$$

Finally, the mover slot permeance is equal to:

$$\rho_{MS}=\frac{\mu_0 h_{MT} w_{MT}}{\frac{l}{N_M}-w_{MT}} \tag{9}$$

where N_M is the number of mover slots in the x or y direction. In order to calculate the air-gap permeances, it should be considered that these permeances are a function of movers' position in both the x and y directions, in addition to the

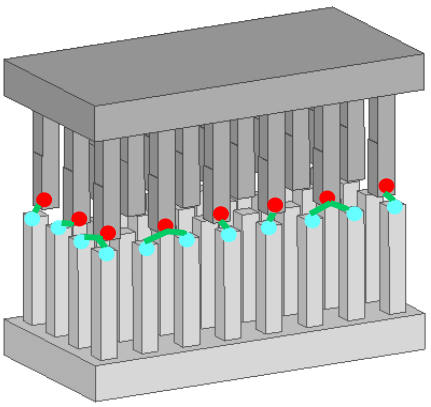

FIGURE 7. The air-gap permeance

geometry of the resolver. Therefore, the equivalent permeance between the mover's i^{th} tooth and the stator's j^{th} tooth is

$$\rho_{ag}(i,j)=\frac{\mu_0 x_c y_c}{g} \quad (10)$$

where x_c and y_c are the overlapping length of the mover's i^{th} tooth with the stator's j^{th} tooth in the x and y directions, respectively.

The superposition principle is employed to solve the proposed equivalent circuit. At first, the magnetomotive force (MMF) of the sources in the x-direction is set equal to zero. In this condition, due to symmetry, the stator nodes with equal x have the same magnetic potential. Therefore, the equivalent circuit in this condition can be the same as that of conventional linear wound mover resolver, except its air-gap length, which is changed due to orthogonal slots. After that, re-employing the superposition principle and turning the y-direction sources off, those sources in Fig. 6(a) can be replaced with a short circuit.

In the proposed circuit, as in the previous state, the nodes of the stator teeth with the equal y-position have the same magnetic potential. Considering the symmetry of resolver structure and the motion in x- or y-directions, the sum of the overlaps between the stator teeth and mover teeth in the other direction is constant. Finally, it is concluded to solve the proposed 3-D MEC model, it is enough to solve the MEC model of the 1-DOF wound mover resolver considering the orthogonal slot effects on the model. Solving Kirchoff's current law (KCL) in each node determines the inductance matrices and the induced voltages in the signal windings as presented in (A1)-(A17).

Fig. 8 shows the block diagram for calculating the signal voltages with the proposed model. The excitation current should be calculated based on the excitation voltage applied to the excitation winding. This is done by assuming R and λ_e as the resistance and the flux linkage of the excitation winding, respectively. The calculated current is applied to the MEC model, and the flux linkages of signal windings are obtained. The signal winding's flux linkages are used to calculate the induced voltages. Then, the envelope of the induced voltages is calculated using peak detection method. Finally, using the inverse tangent of the ratio between the sine and cosine signal voltage envelopes, the mover position is determined as:

$$x = \frac{\tau}{\pi}\, tan^{-1}\left(\frac{envelope\ of\ V_S}{nvelope\ of\ V_C}\right) \quad (11)$$

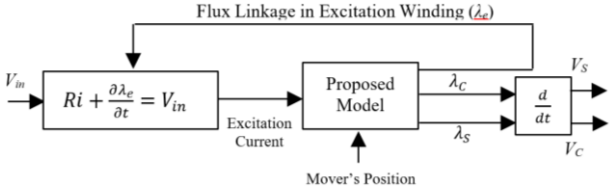

FIGURE 8. Block diagram for calculating the signal voltages using the proposed analytical method

where τ is pole pitch. Then, the position error is determined based on the comparison of the calculated position with the real position.

IV. MODEL VERIFICATION

In this section, the output voltages are calculated employing the proposed analytical model. The output voltages are also obtained from 3-D time stepping finite element method (TSFEM). The performance of the proposed model is studied by comparing its results with those of 3-D TSFEM. Since the MEC model is developed supposing independent operation of each DOF, to ensure the correctness of that assumption, the movement in TSFEM is applied to the mover along the diagonal direction of the stator. The induced voltages in the signal windings of x- and y- directions are given in Figs. 9(a) and (b), respectively. There is close agreement between the results for the MEC model, which evaluated motion in the x- and y-directions independently, and the TSFEM, which evaluated motion in the x- and y-directions simultaneously.

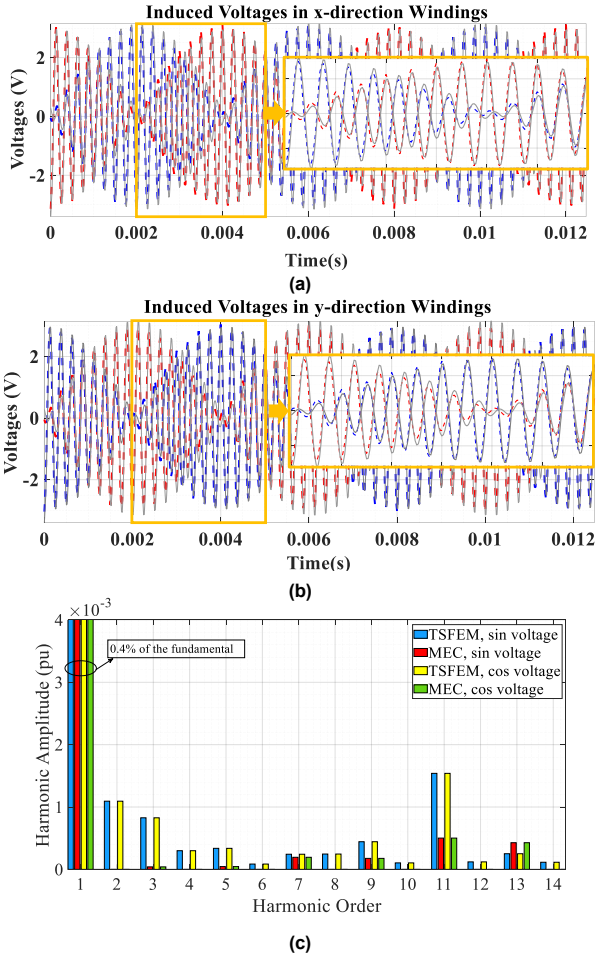

FIGURE 9. Comparing the results of the TSFEM and those of proposed model (solid lines: MEC, dash lines: TSFEM) (a) voltages of x-direction windings, (b) voltages of y-direction windings, and (c) harmonic content of the envelopes (the average of x- and y-direction signals)

Then, the envelope of the amplitude modulated voltages is determined using the peak detection method, and the inverse tangent of the voltages' ratio gives the calculated position. Comparing the calculated position with the actual position gives the position error of the sensor, which is shown in Fig. 10. Comparing the results of the proposed analytical model and those of the 3-D TSFEM method, it can be seen that:

- The assumption of independence between x-direction windings and y-direction windings is correct, and the calculated voltages using the proposed model are in close agreement with those of 3-D TSFEM. The envelope of the MEC voltages has almost the same amplitude (3.07 V) as that of TSFEM (3.15 V for x-direction windings and 2.95 for y-direction windings).
- The model can be used to determine the optimal slot combinations of the stator and mover for different number of poles. Using the model for calculating the position error of the 2-pole resolver (Table 1), approves the success of the selected combination for the stator and mover teeth.
- The AAPE is found by taking the absolute values of the curves in Fig. 10 and then taking the averages with respect to the real position. This is calculated using the developed model equal to 6.5 µm and using TSFEM equal to 7.2 µm and 7.1 µm for the x-and y-directions, respectively. Thus, the difference between the AAPEs predicted by the MEC and by TSFEM is less than 10%. Therefore, the accuracy of the proposed model is almost entirely acceptable while the computational burden of the developed model (4.8 sec.) is orders of magnitude less than that of TSFEM (144 hours).
- The proposed model is developed as a parametric model and can, thus, could be applied to a wide range of designs.
- Finally, considering the accuracy and the computational burden of the proposed model, this model can be involved in iterative design and optimization of the sensor.

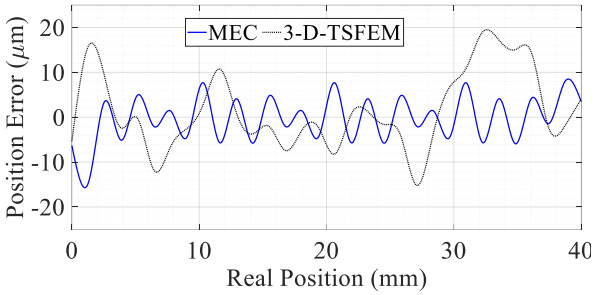

FIGURE 10. The calculated position error using MEC and 3-D TSFEM
Position error of proposed planar resolver

Table 1. The MPE versus different combinations of stator and mover tooth numbers

MPE (µm)		Number of stator teeth				
		8	12	16	20	36
Number of mover teeth	8	83	69	123	49	96
	12	139	58	97	64	84
	16	59	15	134	67	89
	20	39	46	64	57	86
	36	51	47	63	79	45

However, all the simulations above assumed the sensor is infinitely long in the x and y-directions. In practice, both the mover and the stator have finite lengths. Unlike rotating machines, the finite length of the ferromagnetic cores in linear machines leads to an undesirable phenomenon called the longitudinal end effect [16]. In linear resolvers, it causes accuracy deterioration. Therefore, it must be considered in the simulations and compensated for in the design.

V. Longitudinal End Effect

Since the performance of the linear resolver is greatly affected by the longitudinal end effect, the proposed model is

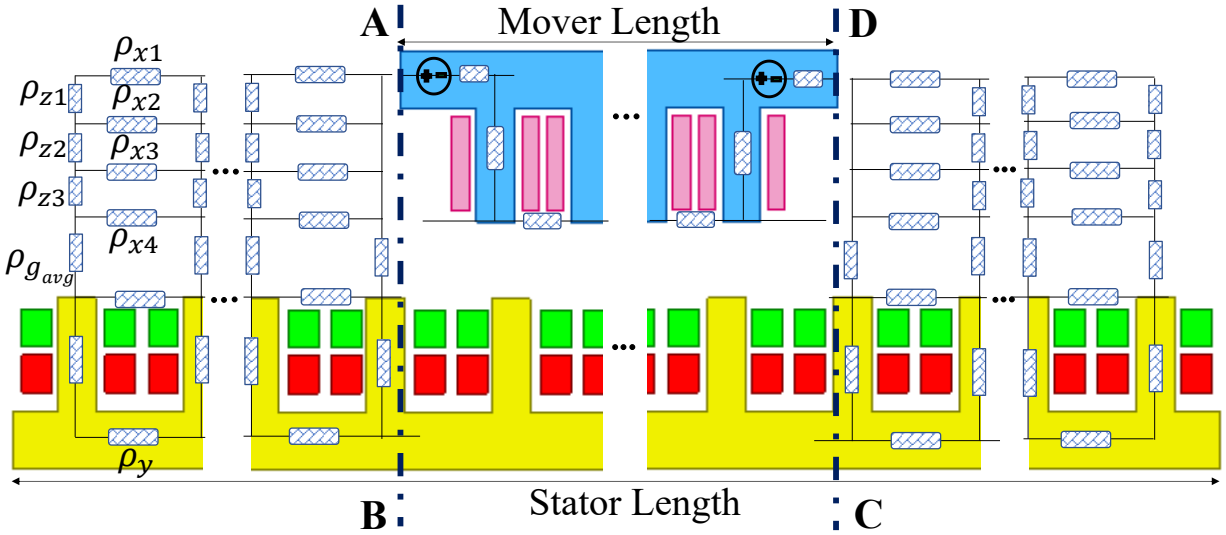

FIGURE 11. Magnetic equivalent circuit considering end effect

improved to evaluate the finite dimensions of the ferromagnetic parts. In this regard, the equivalent permeances of the first and last elements of the air-gap permeance are calculated considering the air instead of iron in the other teeth. In order to model the end effect, at first, a slot pitch of the mover is considered, as shown in Fig. 11. In this slot pitch, the equivalent permeance of the stator and the mover is calculated. Then, a new permeance similar to the previously calculated permeance is added in series, and the equivalent permeance is calculated again. This process is continued until the addition of series blocks does not result in a significant change in the calculated equivalent permeance. Thus, by excluding the permeances of the movers' teeth, the calculated equivalent permeance can be paralleled with the air gap perimeter. This way, the end effect can be adequately studied using the proposed model.

The output voltages considering the influence of the longitudinal end effect are determined using the modified MEC model and the TSFEM and shown in Fig. 12(a). The position error of the sensor using TSFEM and the modified MEC model are presented in Fig. 12(b). The prediction of the modified model is in close agreement with that of TSFEM. As shown in Fig. 12(b), the AAPE of the developed sensor is predicted to be 175 or 194 µm by the modified MEC or the TSFEM, respectively. When ignoring the end effect those values were 6.5 and 7.1 µm.

Thus, the accuracy of the developed sensor is remarkably deteriorated due to the longitudinal end effect. Therefore, it is necessary to propose a compensation method for the longitudinal end effect. In this paper, the proposed method

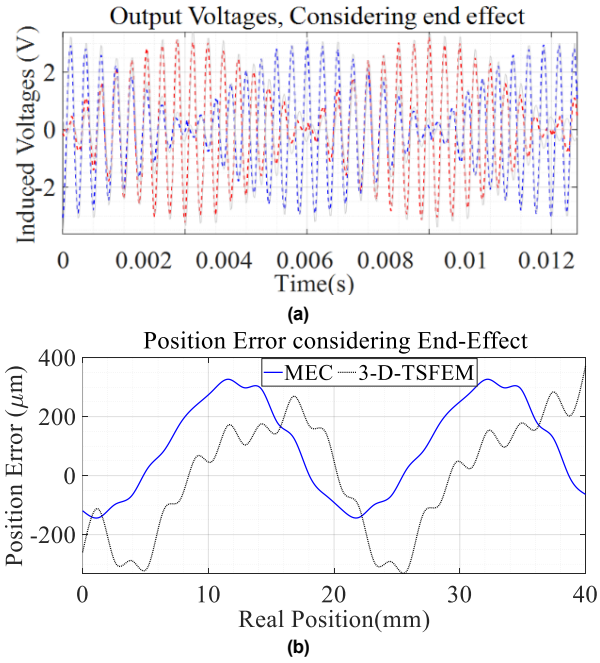

FIGURE 12. **Resolver's output characteristics considering longitude end effect (solid lines are results of the proposed MEC model and the dashed lines are the results of TSFEM): (a) induced voltages, and (b) position error**

adds additional teeth to the ends of the mover in each direction and modifies the turn number of the excitation winding in the end teeth. In order to compensate for the end effect, a synchronized optimization is performed on the width of the added teeth and the coil turn numbers of two lateral teeth. Initially, the tooth width increase is selected to be 10% of the width of the main teeth. Afterward, the change in the number of turns for the first tooth is varied from -20 turns to +20 turns in steps of 5 turns. Finally, the tooth width is increased by steps of 10% to the point that other parameters are also optimized, and the compensation process is completed. Based on the performed optimization, the best optimized design parameters came out to be a 40% increase in the width of the first and last teeth, and also 80 and 75 turns for the excitation coils on the first and last teeth, respectively. (The initial numbers of those turns were 70 and 65, respectively.)

The induced voltages in the signal windings after the proposed compensation method are shown in Fig. 13(a), and the relevant position error is given in Fig. 13(b). As shown in Fig. 13(b), using the proposed compensation method, the AAPE was reduced to 45.4 µm showing a 74% improvement with respect to that of the uncompensated sensor. For better comparison, the position error of the sensor calculated by MEC model, without end effect, with end-effect before compensation, and with end-effect after compensation is shown in Fig. 13(c).

VI. EXPERIMENTAL MEASUREMENT

In this section, the developed sensor is experimentally built and tested to verify the proposed model and the composition method. The stator and the mover core before winding are shown in Figs. 14(a), and (b), respectively. The orthogonal slots necessitated the use of electrostatic powder paint for insulation rather than conventional insulations such as Presspahn Papers. Figs. 14(c) and 14(d) show the cores during the winding. The primary requirement of the test setup was its ability to generate diagonal or straight-line motion and fix the air-gap length at the desired value. The setup in Fig. 14(e) is equipped with three motors; two for diagonal or straight-line motion and a third to keep the air-gap length constant. Motion in each degree of freedom (DOF) is supported by an electrical motor that can generate steps of 1 µm. For diagonal motion, both the x- and y-direction motors must operate at the same speed. To achieve this level of precision, the test room temperature must be maintained at 25 °C. Higher velocities can be achieved by increasing the motion pitch of the servomechanism.

A digitally synthesized function generator was employed to provide the excitation windings with 4 kHz sinusoidal voltage. Subsequently, the induced voltages in the signal windings were captured using a digital oscilloscope and saved as shown

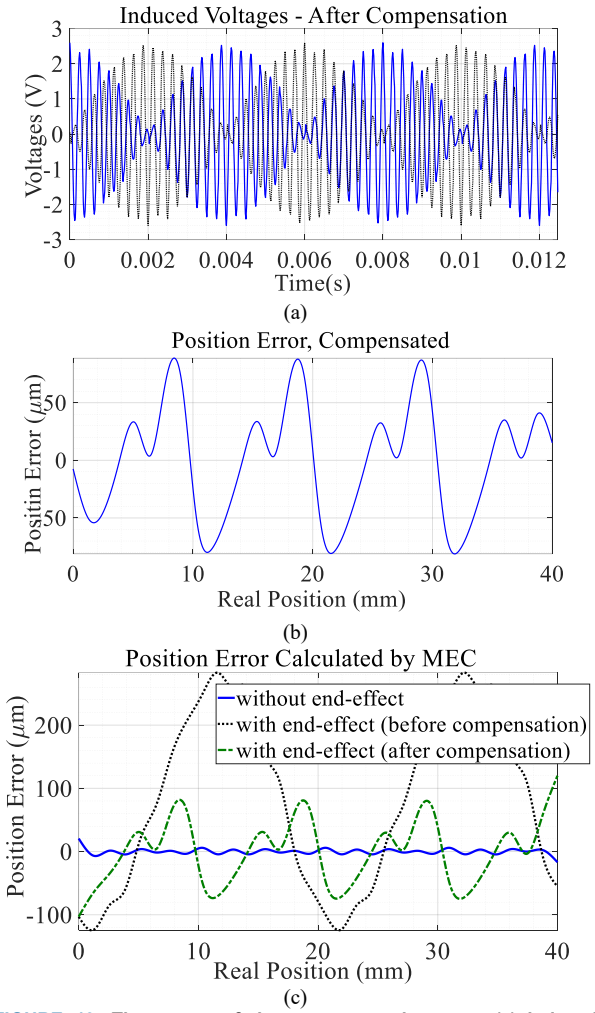

FIGURE 13. The output of the compensated sensor: (a) induced voltages in signal windings, (b) the position error of the sensor, and (c) the position error of the sensor calculated by MEC model, without end effect, with end-effect before compensation, and with end-effect after compensation

in Figs. 15(a) and (b). It is worth mentioning that to consider the uncertainty of the experimental test, the measurements are repeated 10 times and the induced voltages are saved. The results of different measurements are very close to each other that approves the high repeatability of the sensor. MATLAB was then used to decouple the high-frequency carrier and low-frequency envelopes. The ratio of the envelopes was used to determine the position of the mover.

The ratio of the envelopes is used to determine the position of the mover. The AAPE of the sensor considering planar motion is 51 μm and 50 μm, respectively. The predicted value using the proposed model is 45.4 μm. The deviation of the developed model's result from the experimental one is less than 11%. Therefore, the success of the proposed model and the developed accuracy improvement procedure are verified by the measurements on the built sensor.

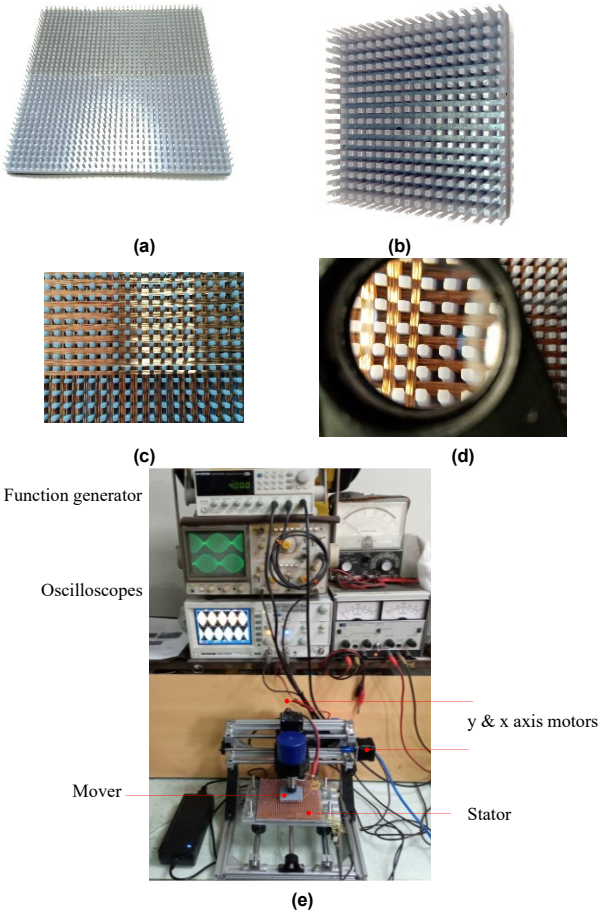

FIGURE 14. Experimental prototype: (a) the insulated stator core, (b) the insulated mover core, (c) the stator core during winding, (d) the mover core during winding, and (e) the developed test circuit

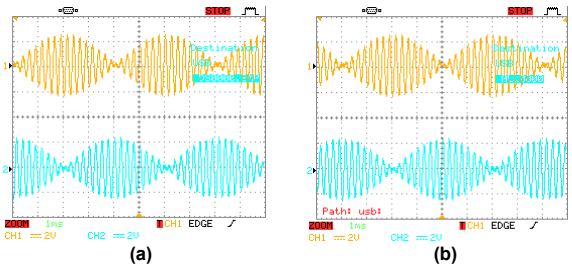

FIGURE 15. The measured voltages in (a) the x-axis windings and (b) the y-axis windings

VII. CONCLUSION

In this paper, a 2-DOF planar resolver is studied, and its operation principle is described. A linear analytical model based on a magnetic equivalent circuit (MEC) is presented for a two-DOF linear planar resolver. The proposed model was modified to consider the finite dimensions of the ferromagnetic core and longitudinal end effects. The accuracy of the model is approved using 3-D TSFEM. Then, the developed model is employed to determine a compensation method for the longitudinal end effect. The proposed compensation method is based on a synchronized optimization of the width of the added mover's end tooth and also the number of turns on the first and last teeth of the excitation coil.

The accuracy of the optimized sensor is improved by 74% with respect to the uncompensated sensor.

Finally, the compensated sensor is experimentally built and tested to verify the accuracy of the developed model. The accuracy of the developed model is comparable with that of TSFEM, while its computational load was much less than that of TSFEM. The discrepancy between the experimental AAPE and that predicted by the proposed MEC model is less than 11%.

APPENDIX

The induced voltages in the signal windings can be determined as:

$$v_s = \frac{d\lambda_s}{dt} \tag{A1}$$

$$v_c = \frac{d\lambda_c}{dt} \tag{A2}$$

where v_s/v_c is the induced voltage in sin/cos signal winding and λ_s/λ_c is the flux linkage of the sin/cos windings:

$$\lambda_s = [T_s] \times [\varphi_{ST}] \tag{A3}$$

$$\lambda_c = [T_c] \times [\varphi_{ST}] \tag{A4}$$

where T_S and T_C are the turn number of sin and cos coils on each stator tooth and φ_{ST} is the magnetic flux that passes through the same stator tooth and can be calculated as (A5).

In (A5) A_{ST}/A_{SY} is the electromagnetic potential of stator's tooth/yoke and those of mover's tooth/yoke are A_{MT}/A_{MY}. Then, the matrix of the electromagnetic potential can be determined as:

$$A = [[A_{MY}] \quad [A_{MT}] \quad [A_{ST}] \quad [A_{SY}]]^T \tag{A6}$$

$$A = M^{-1} \times \begin{bmatrix} 0 \\ [\mathcal{F}_{MT}] \end{bmatrix} \tag{A7}$$

where $\mathcal{F}_{MT}$ is the magnetomotive force and can be calculated as:

$$[\mathcal{F}_{MT}] = [T]i \tag{A8}$$

where i denotes the excitation current and T the turn number of the excitation winding.

$[M]$ in (A7) can be written as (A9) and the matrix elements are defined as (A10)-(A17).

$$[\varphi_{ST}] = [M_{SYST}] \times ([A_{ST}] - [A_{SY}]) = \begin{bmatrix} \rho_{TSU}+\rho_{TSD} & 0 & & 0 & 0 \\ 0 & \rho_{TSU}+\rho_{TSD} & & 0 & 0 \\ 0 & 0 & \ddots & 0 & 0 \\ 0 & 0 & & \rho_{TSU}+\rho_{TSD} & 0 \\ 0 & 0 & & 0 & \rho_{TSU}+\rho_{TSD} \end{bmatrix} \times ([A_{ST}] - [A_{SY}]) \tag{A5}$$

$$M = \begin{bmatrix} [M_{MY}] & -[M_{MYMT}] & 0 & 0 \\ -[M_{MYMT}] & [M_{MT}]+[M_{STMT}] & -[\rho_{ag}]^T & 0 \\ 0 & -[\rho_{ag}] & [M_{ST}]+[M_{STMT}] & [M_{SYST}] \\ 0 & 0 & -[M_{SYST}] & [M_{SY}] \end{bmatrix} \tag{A9}$$

$$[M_{SY}] = \begin{bmatrix} 2\rho_{SY}+\rho_{TSU}+\rho_{TSD} & -\rho_{SY} & 0 & & 0 & 0 & -\rho_{SY} \\ -\rho_{SY} & 2\rho_{SY}+\rho_{TSU}+\rho_{TSD} & -\rho_{SY} & & 0 & 0 & 0 \\ & & & \ddots & & & \\ 0 & 0 & 0 & & -\rho_{SY} & 2\rho_{SY}+\rho_{ST}+\rho_{TSD} & -\rho_{SY} \\ -\rho_{SY} & 0 & 0 & & 0 & -\rho_{SY} & 2\rho_{SY}+\rho_{TSU}+\rho_{TSD} \end{bmatrix} \tag{A10}$$

$$[M_{SYST}] = \begin{bmatrix} \rho_{TSU}+\rho_{TSD} & 0 & & 0 & 0 \\ 0 & \rho_{TSU}+\rho_{TSD} & & 0 & 0 \\ 0 & 0 & \ddots & 0 & 0 \\ 0 & 0 & & \rho_{TSU}+\rho_{TSD} & 0 \\ 0 & 0 & & 0 & \rho_{TSU}+\rho_{TSD} \end{bmatrix} \tag{A11}$$

$$[M_{MYMT}] = \begin{bmatrix} \rho_{TMU}+\rho_{TMD} & 0 & & 0 & 0 \\ 0 & \rho_{TMU}+\rho_{TMD} & & 0 & 0 \\ 0 & 0 & \ddots & 0 & 0 \\ 0 & 0 & & \rho_{TMU}+\rho_{TMD} & 0 \\ 0 & 0 & & 0 & \rho_{TMU}+\rho_{TMD} \end{bmatrix} \tag{A12}$$

$$[M_{STMT}] = \begin{bmatrix} \sum_{i=1}^{N_s} \rho_{ag}(i,1) & 0 & 0 \\ 0 & \sum_{i=1}^{N_s} \rho_{ag}(i,2) & 0 \\ & & \ddots \\ 0 & 0 & \sum_{i=1}^{N_s} \rho_{ag}(i,N_m) \end{bmatrix} \tag{A13}$$

$$[M_{ST}] = \begin{bmatrix} 2\rho_{ss}+\rho_{TSU}+\rho_{TSD} & -\rho_{ss} & 0 & 0 & 0 & -\rho_{ss} \\ -\rho_{ss} & 2\rho_{ss}+\rho_{TSU}+\rho_{TSD} & -\rho_{ss} & 0 & 0 & 0 \\ & & & \ddots & & \\ 0 & 0 & 0 & -\rho_{ss} & 2\rho_{ss}+\rho_{TSU}+\rho_{TSD} & -\rho_{ss} \\ -\rho_{ss} & 0 & 0 & 0 & -\rho_{ss} & 2\rho_{ss}+\rho_{TSU}+\rho_{TSD} \end{bmatrix} \tag{A14}$$

$$[M_{MY}] = \begin{bmatrix} 2\rho_{ym}+\rho_{TMU}+\rho_{TMD} & -\rho_{yr} & 0 & 0 & 0 & -\rho_{ym} \\ -\rho_{ym} & 2\rho_{ym}+\rho_{TMU}+\rho_{TMD} & -\rho_{ym} & 0 & 0 & 0 \\ & & & \ddots & & \\ 0 & 0 & 0 & -\rho_{ym} & 2\rho_{ym}+\rho_{TMU}+\rho_{TMD} & -\rho_{ym} \\ -\rho_{yr} & 0 & 0 & 0 & -\rho_{ym} & 2\rho_{ym}+\rho_{TMU}+\rho_{TMD} \end{bmatrix} \tag{A15}$$

$$[M_{MT}] = \begin{bmatrix} 2\rho_{sm}+\rho_{TMU}+\rho_{TMD} & -\rho_{sm} & 0 & 0 & 0 & -\rho_{sm} \\ -\rho_{sm} & 2\rho_{sm}+\rho_{TMU}+\rho_{TMD} & -\rho_{sm} & 0 & 0 & 0 \\ & & & \ddots & & \\ 0 & 0 & 0 & -\rho_{sm} & 2\rho_{sm}+\rho_{TMU}+\rho_{TMD} & -\rho_{sm} \\ -\rho_{sm} & 0 & 0 & 0 & -\rho_{sm} & 2\rho_{sm}+\rho_{TMU}+\rho_{TMD} \end{bmatrix} \tag{A16}$$

$$[\rho_{ag}] = \begin{bmatrix} \rho_{ag}(1,1) & \rho_{ag}(1,2) & \rho_{ag}(1,3) & \rho_{ag}(1,N_m) \\ \rho_{ag}(2,1) & \rho_{ag}(2,2) & \rho_{ag}(2,3) & \rho_{ag}(2,N_m) \\ \rho_{ag}(3,1) & \rho_{ag}(3,2) & \rho_{ag}(3,3) & \rho_{ag}(3,N_m) \\ & & \ddots & \\ \rho_{ag}(N_s,1) & \rho_{ag}(N_s,2) & \rho_{ag}(N_s,3) & \rho_{ag}(N_s,N_m) \end{bmatrix} \tag{A17}$$

REFERENCES

[1] A. Keyvannia and Z. Nasiri-Gheidari, "A Comprehensive Winding Method for Linear Variable-Reluctance Resolvers to Compensate for the End Effects," *IEEE Trans. Ind. Electron*, vol. 70, no. 9, pp. 9593-9600, Sep. 2023, doi: 10.1109/TIE.2022.3210572.

[2] S. Jikai, X. Lujia, X. Xiaozhuo, Z. Yifeng, C. Wenping, "Static coupling effect of a two-degree-of-freedom direct drive induction motor", *IET Electr. Power Appl.*, vol. 11, no. 4, pp. 532-539, Apr. 2017.

[3] A. Paymozd, H. Saneie, A. Daniar and Z. Nasiri-Gheidari, "Accurate and Fast Subdomain Model for Electromagnetic Design Purpose of Wound-Field Linear Resolver," *IEEE Trans. Instrnm. Meas.,* vol. 70, pp. 1-8, 2021,

[4] M. KhajueeZadeh, H. Saneie and Z. Nasiri-Gheidari, "Development of a Hybrid Reference Model for Performance Evaluation of Resolvers," *IEEE Trans. Instrnm. Meas.,*, vol. 70, pp. 1-8, 2021.

[5] H. Tsujimoto, S. Tanaka, T. Shimono, T. Mizoguchi, M. Watanabe, K. Ishikawa, "Design and Analysis of a Resolver for 2DOF Tubular Motor", *IECON 2016 - 42nd Annual Conference of the IEEE Industrial Electronics Society*, Florence, Italy, 23-26 Oct. 2016.

[6] F. Zare and Z. Nasiri-Gheidari, "Proposal of a 2DOF Wound-Rotor Resolver," *IEEE Sensors J.*, vol. 21, no. 17, pp. 18633-18640, Sept. 2021.

[7] A. Ortega–Vidal, F. Salazar–Vasquez and A. Rojas–Moreno, "A comparison between optimal LQR control and LQR predictive control of a planar robot of 2DOF," *2020 IEEE XXVII International Conference on Electronics, Electrical Engineering and Computing (INTERCON)*, 2020, pp. 1-4, doi: 10.1109/INTERCON50315.2020.9220263.

[8] Y. Ihn, "Two-DOF actuator module design and development based on fully decoupled parallel structure", *Microsyst. Technol.*, vol. 24 pp. 1359-1368, 2018.

[9] P. Naderi, R. Ghandehari and M. Heidary, "A Comprehensive Analysis on the Healthy and Faulty Two Types VR-Resolvers with Eccentricity and Inter-Turn Faults," *IEEE Trans. Energy Convers.*, vol. 36, no. 4, pp. 3502-3511, Dec. 2021, doi: 10.1109/TEC.2021.3079725.

[10] A. Paymozd, H. Saneie, Z. Nasiri-Gheidari and F. Tootoonchian, "Subdomain Model for Predicting the Performance of Linear Resolver Considering End Effect and Slotting Effect," *IEEE Sensors J.*, vol. 20, no. 24, pp. 14747-14755, Dec. 2020.

[11] Y. Hojjat, "Development of an inductive encoder for simultaneous measurement of two-dimensional displacement", *Int. J. Adv. Manuf. Technol.*, vol. 53, pp. 681-688, Aug. 2011.

[12] R. Faryadras and F. Tootoonchian, "Design and Experimental Investigation of a Two-DOF Planar Resolver," *IEEE Trans. Instrnm. Meas.,* vol. 71, pp. 1-8, 2022.

[13] X. Gel, and Z.Q. Zhu, "A Novel Design of Rotor Contour for Variable Reluctance Resolver by Injecting Auxiliary Air-Gap Permeance Harmonics", *IEEE Trans. Energy Convers.*, vol. 31, no. 1, pp. 345-353, Feb. 2016.

[14] R. Alipour-Sarabi, Z. Nasiri-Gheidari, F. Tootoonchian and H. Oraee, "Effects of Physical Parameters on the Accuracy of Axial Flux Resolvers," *IEEE Trans. Magn.,* vol. 53, no. 4, pp. 1-11, April 2017, Art no. 8101211, doi: 10.1109/TMAG.2016.2645163.

[15] P. Naderi, R. Ghandehari and M. Heidary, "A Comprehensive

Analysis on the Healthy and Faulty Two Types VR-Resolvers with Eccentricity and Inter-Turn Faults," *IEEE Trans. Energy Convers.*, vol. 36, no. 4, pp. 3502-3511, Dec. 2021.

[16] A. Paymozd, H. Saneie, Z. Nasiri-Gheidari and F. Tootoonchian, "Subdomain Model for Predicting the Performance of Linear Resolver Considering End Effect and Slotting Effect," *IEEE Sensors J.*, vol. 20, no. 24, pp. 14747-14755, Dec. 2020.

Fateme Zare received the B.Sc. degree in electrical engineering from the Sharif University of Technology, Tehran, Iran, in 2016, the M.Sc. degree in electrical engineering from Isfahan University of Technology, Isfahan, Iran, in 2018, and the Ph.D. degree in electrical engineering from the Sharif University of Technology, Tehran, Iran, in 2022. She is currently an Assistant Professor at the Department of Electrical and Computer Engineering, Isfahan University of Technology. Her research interests include design and optimization of electrical machines and electromagnetic sensors.

Farid Tootoonchian received the B.Sc. and M.Sc. degrees in Electrical Engineering from the Iran University of Science and Technology, Tehran, Iran, in 2000 and 2007, respectively, and the Ph.D. degree from the K. N. Toosi University of Technology, Tehran, in 2012, all in electrical engineering. He is currently an Associate Professor at the Department of Electrical Engineering, Iran University of Sciences and Technology. His research interests include design, optimization, finite-element analysis, and prototyping of ultrahigh-speed electrical machines and ultrahigh-precision electromagnetic sensors.

Ahmad Daniar (S'20) earned his B.Sc. degree in electrical engineering from the University of Tabriz, Tabriz, Iran, in 2014, and the M.Sc. degree in electrical engineering from Sharif University of Technology, Tehran, Iran, in 2017. He is currently working toward his Ph.D. degree in electrical engineering with The University of Texas at Dallas, Richardson, TX, USA. His research interests include design, modelling, optimization, and control of electric machines and power converters.

Matthew C. Gardner (S' 15, M' 19) earned his B.S. in electrical engineering from Baylor University, Waco, Texas in 2014. He earned his Ph.D. in electrical engineering from Texas A&M University, College Station, Texas in 2019. In 2020, he joined the University of Texas at Dallas, Richardson, Texas as an assistant professor of electrical and computer engineering. His research interests include optimal design and control of electric machines, magnetic gears, and electromagnetic devices.

Bilal Akin (Fellow Member, IEEE) received the Ph.D. degree in electrical engineering from Texas A&M University, College Station, TX, USA, in 2007. From 2005 to 2008, he was a Research and Development Engineer with Toshiba Industrial Corporation, Houston, TX, USA. From 2008 to 2012, he was a Research and Development Engineer with C2000 DSP Systems, Texas Instruments Inc., Houston, TX, USA. Since 2012, he has been a Faculty Member with The University of Texas at Dallas, Richardson, TX, USA. His research interests include design, control, and diagnosis of electric motors and drives, digital power control, and management, and fault diagnosis and condition monitoring of power electronics components and ac motors.

Dr. Akin was the recipient of the NSF CAREER 2015 Award, two IEEE Transactions on Industry Applications Prize Paper Awards, Top Editors Recognition Award from the IEEE Transactions on Vehicular Technology Society, Jonsson School Faculty Research Award twice, and Jonsson School Faculty Teaching Award. He is currently the Co-Editor-in-Chief of the IEEE Transactions on Vehicular Technology.